Simultaneous precipitation of magnesite and lizardite from hydrothermal alteration of olivine under high-carbonate alkalinity

Romain Lafay, German Montes-Hernandez, Emilie Janots, Nathaniel Findling, Rodica Chiriac, Francois Toche

Simultaneous precipitation of magnesite and lizardite from hydrothermal alteration of olivine under high-carbonate alkalinity

Romain Lafay[a, b], German Montes-Hernandez[a, *], Emilie Janots[b], Rodica Chiriac[c], Nathaniel Findling[b], François Toche[c]

[a] CNRS, ISTerre, F-38041 Grenoble, France

[b] Univ. Grenoble Alpes, ISTerre, F-38041 Grenoble, France

[c] Université de Lyon, Université Lyon 1, Laboratoire des Multimatériaux et Interfaces UMR CNRS 5615, 43 bd du 11 novembre 1918, 69622 Villeurbanne Cedex, France

*Corresponding author: G. Montes-Hernandez

E-mail address: german.montes-hernandez@ujf-grenoble.fr

Abstract

The present study reports original experiments in order to investigate the simultaneous serpentinization and carbonation of olivine with relevance in Earth systems (e.g. functioning of hydrothermal fields) or in engineered systems (e.g. ex-situ and in-situ mineral sequestration of CO_2). For this case, specific experimental conditions were examined (200°C, saturated vapor pressure ≈ 16bar, solution/solid weight ratio = 15, olivine grain size < 30µm and high-carbonate alkalinity ≈ 1M $NaHCO_3$). Under these conditions, competitive precipitation of magnesite and serpentine (preferentially lizardite type) were clearly determined by using conventional analytic tools (XRD, FESEM, FTIR and TGA); excluding the fate of the iron initially contained in olivine, the alteration reaction for olivine under high-carbonate alkalinity can be expressed as follows:

$$2Mg_2SiO_4 + 2H_2O + HCO_3^- \rightarrow MgCO_3 + Mg_3Si_2O_5(OH)_4 + OH^-$$

This reaction mechanism implied a dissolution process, releasing Mg and Si ions into solution until supersaturation of solution with respect to magnesite and/or serpentine. The released iron contained in the olivine has not implied any precipitation of iron oxides or (oxy)hydroxides; in fact, the released iron was partially oxidized (about 50%) via a simple reduction of water ($2Fe^{2+} + 2H_2O \rightarrow 2Fe^{3+} + H_2 + 2OH^-$). In this way, the released iron was incorporated in serpentine (Fe(II) and Fe(III)) and in magnesite (Fe(II). This latter was clearly determined by FESEM/EDS chemical analysis on the single magnesite crystals. The nucleation and epitaxial growth processes at the olivine-fluid interfaces cannot be excluded in our investigated system.

The experimental kinetic data fitted by using a kinetic pseudo-second-order model have revealed

a retarding process of serpentine formation with respect to magnesite (about three times slower); in fact, the magnesite seems to reach an apparent stabilization after about 20 days of reaction while the serpentine follows a progressive slower evolution. We assumed that the magnesite has reached a fast apparent equilibrium with solution because the available carbonate species are not renewed from fluid phase as typically constrained in aqueous carbonation experiments where a given CO_2 pressure is imposed in the system.

On the other hand, the reactivity of serpentinized olivine (chrysotile+brucite+small amount of residual olivine) and high-purity chrysotile at the same above investigated conditions; and the olivine serpentinization in initial acid pH ≈ 0.66 are also reported as complementary information in this study.

These novel experimental results concerning simultaneous serpentinization and aqueous carbonation of olivine expand the thermodynamic conditions where serpentine and magnesite can simultaneously precipitate; this could contribute to a better understanding of fluid-rock interactions in natural active hydrothermal fields on Earth.

Keywords: Olivine alteration; High-carbonate alkalinity; Magnesite; Lizardite; Crystal growth; Hydrothermal systems.

1. Introduction

The physicochemical reactions at the solid-fluid interfaces play a crucial role in the global cycle of major and trace elements in the Earth and other telluric planets. In this way, chemical weathering, metamorphic reactions, diagenetic reactions, hydrothermalism, volcanic activity, crystal-melt reactions are important non-limited physicochemical processes that shape the Earth's surface and sub-surface. However, many physicochemical and textural aspects of these so-called rock-fluid interactions are still poorly understood. For example, when mantle peridotite is tectonically exposed with (sub-) surface fluids (e.g. seafloor water and meteoric water), the olivine and pyroxene anhydrous minerals contained in peridotite are far-from-equilibrium with respect to fluid composition. In this way, numerous physicochemical reactions at peridotite-fluid interfaces can take place such as hydration (-OH incorporation or serpentinization) and carbonation processes if the required temperature and fluid compositions are enough to activate these reactions; both most important processes directly related to natural H_2 and abiotic methane production via redox reactions and the formation of other non-limited secondary minerals as it has been observed in various natural hydrothermal sites (e.g. Logatchev, Rainbow, The Lost City...) (e.g. Charlou et al., 2002; Allen and Seyfried, 2004; Ludwig et al., 2006; Seyfried Jr. et al., 2007; McCollom and Bach 2009; Klein et al., 2009 ; Rudge et al., 2010 ; Seyfried Jr., et al., 2011). Such reducing systems may represent analogues to early Earth environments and may provide insights into requirements for the emergence of life, probably initiated at the sea floor (e.g. MacLeod et al., 1994; Charlou et al., 2002; Früh-Green et al., 2003; Kelley et al., 2005). The field monitoring and ex-situ characterization have revealed complex fluid chemistry and generally low pH (from 2.8 to 4.3) and high temperature (from 275 to 365°C) in the expelled

fluids from various studied ultramafic-hosted hydrothermal systems at the Mid-Atlantic Ridge (Charlou et al., 2002). Conversely, the expelled fluids at the Lost City field and other sites for example in continental serpentinization systems (e.g. Samail Ophiolite in Oman) are highly alkaline (pH>9) and lower temperatures have been monitored/determined (from 55 to 90°C) (Kelley et al., 2001; Früh-Green et al., 2003; Ludwig et al., 2006; Kelemen et al., 2011). These surprising measurements and the recent discovery of spectacular carbonate towers at the Lost City hydrothermal field have stimulated interest in the role of serpentinization and carbonation processes on the production of hydrogen- and methane-rich fluids and on the biological communities that may be supported in these environments (Früh-Green et al., 2003; Kelley et al., 2005; Schrenk et al., 2013). Moreover, at the present time, the ex-situ and in-situ carbonation of mafic and ultramafic rocks (e.g. basalts and peridotite), extensively available in the oceanic crust and ophiolites, have been proposed as a promising solution to mitigate the global warming of Earth's atmosphere related to excessive anthropogenic and natural CO_2 emissions; because Mg-Ca- or Fe-carbonates resulting from mineral carbonation of CO_2 can remain stable at the geological time scales as frequently observed in the Earth surface and/or sub-surface (e.g. Seifritz, 1990; Lackner et al., 1995; Bachu, 2000; Kaszuba et al., 2003; Xu et al., 2004, Kaszuba et al., 2005; IPCC, 2007; Gerdemann et al., 2007; Kelemen and Matter, 2008; Oelkers et al., 2008; Montes-Hernandez et al., 2009; Matter and Kelemen, 2009; Kelemen et al., 2011; Schwarzenbach et al., 2013). In this general context, numerous experimental studies concerning the serpentinization or carbonation of peridotite (or single olivine) have been recently performed using batch, semi-continuous or flow-through reactors in order to better understand the reaction mechanisms and kinetics, reaction and cracking propagation from the grain boundaries, nature and role of secondary phase formation, potential of hydrogen production, potential for mineral

114 sequestration of CO_2 and role of P, T, pH, solid/fluid ratio and fluid chemistry (e.g. Wunder and
115 Schreyer, 1997; James et al., 2003; Giammar et al.; 2005; Béarat et al., 2006; Seyfried Jr. et al.,
116 2007; Andreani et al., 2009; McCollom and Bach, 2009; King et al., 2010; Garcia et al., 2010;
117 Daval et al., 2011; Hövelmann et al., 2011; Marcaillou et al., 2011; Klein and Garrido, 2011;
118 Bonfils et al., 2012; Malvoisin et al., 2012; Lafay et al., 2012). However, the competitive and/or
119 coexistence between serpentinization and carbonation at peridotite-fluid interfaces have been
120 rarely investigated at the laboratory scale, remarking that serpentinization and carbonation of
121 peridotite, leading to precipitation of serpentine (e.g. lizardite, chrysotile…) and magnesite (or
122 hydrated Mg carbonates), could occur simultaneously in natural hydrothermal systems if the
123 interacting solution is supersaturated with respect to both minerals. For this simple reason, the
124 main goal of this present study was focussed to determine the simultaneous precipitation of
125 serpentine and magnesite from hydrothermal alteration of olivine under high-carbonate alkalinity.
126 For this particular case, specific experimental conditions were used (200°C, saturation vapour
127 pressure (≈16bar), solution/solid weight ratio (=15), olivine grain size (<30µm) and high-
128 carbonate alkalinity solution (1M $NaHCO_3$)). These experimental conditions were selected with
129 help of previous-experimental studies, investigating independently the serpentinization or the
130 carbonation of olivine (e.g. Giammar et al.; 2005; Béarat et al., 2006; Seyfried Jr. et al., 2007;
131 King et al., 2010; Garcia et al., 2010; Daval et al., 2011; Hövelmann et al., 2011; Marcaillou et
132 al., 2011; Bonfils et al., 2012; Malvoisin et al., 2012; Lafay et al., 2012). High-purity synthetic
133 chrysotile and serpentinized olivine (chrysotile + brucite mineral + small amount of residual
134 olivine) obtained in our laboratory were also used as starting solids in complementary-similar
135 experiments in order to determine their reactivity under high-alkalinity. As expected, the
136 chrysotile was slightly altered and brucite quickly transformed to magnesite at the investigated

conditions. Various analytical tools such as X-ray diffraction (XRD), Field Emission Gun Scanning Electron Microscopy (FESEM), Thermogravimetric analyses (TGA/SDTA) and Fourier Transform Infrared Spectroscopy (FTIR) were used to characterize the solid products. TGA analyses and the respective 1st derivative curves were particularly used to determine with high accuracy the temporal variation of magnesite and serpentine during olivine alteration.

2. Materials and Methods

2.1. Preparation of solid reactants

Olivine grains: Millimetric grains of olivine San Carlos (Fo_{91}) were crushed using a Fritsh Pulverisette 7 micro-crusher. One class of grain/particle size (particle size<30 µm) was isolated by sieving. The samples were washed three times using high-pure water in order to remove the ultrafine particles that possibly stuck at grain surfaces during crushing step. Optical and electron microscopy was performed to control the initial state/appearance of olivine surfaces. On the other hand, high specific surface area (2.3 m^2/g) was deduced from N_2 adsorption isotherm using conventional Brunauer–Emmett–Teller (BET) method. This high specific surface area was probably due to a significant presence of very fine particles (<1µm; not verified), not spherical morphology of grains and significant surface-defaults and/or roughness.

High-purity synthetic chrysotile: 250ml of 1M NaOH solution, 1.302g of silica gel (H_2SiO_3) and 5.082g of magnesium chloride hexahydrate ($MgCl_2.6H_2O$) were placed in a Parr *copper alloy* reactor (autoclave with internal volume of 0.5L). This aqueous reactive system was immediately stirred using constant mechanical agitation (300 rpm) during the reaction. The aqueous system

158 was then heated at 300°C for 30h by using a heating jacket adapted to the reactor. Based on
159 several previous experiments, these experimental conditions were optimal to synthesize high-
160 purity chrysotile with high specific surface area (S_{BET} = 185$m^2.g^{-1}$), more specifically a
161 mesoporous material (pore size 2 to 50 nm) (Lafay et al., 2013).

162 *Serpentinized olivine (chrysotile+brucite+small amount of residual olivine):* micrometric grains
163 of olivine (<30µm) were altered in concentrated NaOH solution (1M) at 200°C in static batch
164 mini-reactors for 30 days. 30 days of olivine-fluid interactions were enough to obtain almost
165 complete mineral replacement of olivine to chrysotile and brucite. This implied a spatial and
166 temporal coupling of dissolution and precipitation reactions at the interface between olivine and
167 chrysotile–brucite minerals. This coupled dissolution–precipitation led to the alteration of starting
168 olivine grains (so-called primary or parent mineral) to a porous mineral assemblage of chrysotile
169 and brucite with preservation of the initial olivine grain shape. For more specific details on the
170 olivine replacement by chrysotile and brucite, including kinetics and reaction steps, refer to Lafay
171 et al., (2012).

172

173 *2.2. Preparation of reacting solutions*

174 *High-alkaline $NaHCO_3$ solution (S1):* This alkaline solution was recovered from magnesite
175 synthesis that has used $Mg(OH)_2$ (1mol), NaOH (2mol), high-purity H_2O (1L) and CO_2 (50bar
176 equivalent to 2mol in the reactor) as reactants. More details on this synthesis method and
177 recovery of alkaline solution by centrifugation can be found in Montes-Hernandez et al., (2012).
178 In summary the recovered solution has a pH of 8.9 (measured at ~20°C), a high concentration of

179 total carbon (=1M) measured by TOC-V_{CSN} analyzer and low concentration of Mg (~250mg/L)
180 measured by ICP-OES. Assuming that all dissolved carbon comes from injected CO_2, the
181 Phreeqc equilibrium modeling (Parkhurst and Appelo, 1999) confirms that the recovered solution
182 is enriched particularly with $NaHCO_3$ (~1M).

183 *High-alkaline $NaHCO_3$ solution (S2):* This solution was obtained by direct capture of CO_2 via
184 ionic dissociation in a concentrated NaOH solution (2M). Herein, 50bar of CO_2 (~2mol) were
185 injected into the reaction titanium cell (2L of volume) at ambient temperature (~20°C). The CO_2
186 consumption (or pressure drop of CO_2) and temperature (exothermic reaction) were in-situ
187 monitored until a macroscopic equilibrium that was reached after about 24h. Then, the residual
188 CO_2 gas was removed from reactor and the solution was recovered by simple decanting of
189 supernatant solution. Based on Solvay typical reactions, the following global reactions are
190 expected:

191 $$2NaOH + CO_2 \rightarrow Na_2CO_3 + H_2O \quad (1a)$$

192 $$Na_2CO_3 + H_2O + CO_2 \rightarrow 2NaHCO_3 \quad (1b)$$

193 The X-ray diffraction on the recovered solid and the measurements in the solution (pH=8.7 and
194 TC=0.95M) have confirmed this above reactions.

195

196 *2.3. Serpentinization-Carbonation experiments*

197 In each experiment 1.5 ml of high-alkaline solution (S1 or S2) and 100 mg of olivine (grain
198 size<30µm) were placed in a Teflon cell reaction (cap-cell also in Teflon). Cell reaction and cap-

cell were previously washed by an acidic treatment followed by washing with high-pure water. This cell reaction was immediately assembled into a steel autoclave without agitation, referred to as ‘‘static batch reactor’’ and the closed autoclave was placed in a multi-oven (ten independent-temperature compartments) and heated to 200 °C (P_{sat}≈16bar). Various olivine-fluid reaction times from 3 h to 60 days were considered in order to determine the serpentinization and carbonation rates of olivine at the investigated hydrothermal conditions. Complementary experiments were carried out at the same experimental conditions. Herein, serpentinized olivine (chrysotile+brucite+small amount of residual olivine) was reacted with *S1* solution (runs: 11 to 15) and high-purity synthetic chrysotile was also reacted with *S1* solution (runs: 6 to 10). All experiments or runs and some results are summarized in Table 1.

At the end of the experiment, the autoclave was quenched in cold water and then disassembled. The quenching step avoids a significant perturbation of solid reaction products. Conversely, the chemistry of recovered solutions (pH, ion composition and probably ion speciation) can be significantly modified by cooling and/or depressuring processes as clearly demonstrated by modelling for calcite precipitation under hydrothermal conditions (Fritz et al., 2013). For this reason, the olivine alteration was directly deduced from solid mineral characterization in this present study. Moreover, for batch experiments, the ion composition and/or concentration are not directly related to alteration extent for a given mineral(s). In summary, only the pH into the collected solutions was measured at room temperature (≈20°C) “not representative of in-situ pH during olivine alteration”, these results are also summarized in Table 1. The solid product was systematically washed in 25ml of high-purity water and separated by centrifugation. Finally, the

220 solid product was directly dried in the centrifugation flask at 90 °C for 24 h. The dry solid
221 product was recovered for further solid characterizations described below.

222 *2.4. Serpentinization in initial acid pH*

223 Similar to above alteration procedure was performed to investigate the effect of initial acid pH on
224 the serpentinization process. For this case, the olivine grains (<30µm) were exposed in HCl
225 solution (*S3*) (initial pH=0.63) at different duration times (10, 66, 90 and 180 days). These batch
226 experiments are also summarized in Table 1.

227 *2.5. Characterization of solid products*

228 The following four conventional techniques were used in complementary manner to determine
229 the mineral composition, morphology of crystals and serpentine polymorphs of reacted samples.

230 *FESEM observations:* Serpentinized-carbonated materials were dispersed by ultrasonic treatment
231 in absolute ethanol (chemical purity>98%) for five to ten minutes. One or two droplets of the
232 suspension were then deposited directly on an aluminum support for SEM observations, and
233 coated with platinum. The morphology of various selected powders was observed using a Zeiss
234 Ultra 55 field emission gun scanning electron microscope (FESEM) with a maximum spatial
235 resolution of approximately 1nm at 15kV.
236 *XRD measurements*: X-Ray Powder Diffraction (XRD) analyses were performed using a Siemens
237 D5000 diffractometer in Bragg-Brentano geometry; equipped with a theta-theta goniometer with
238 a rotating sample holder. The XRD patterns were collected using Cu $k\alpha_1$ ($\lambda_{k\alpha1}$=1.5406Å) and $k\alpha_2$
239 ($\lambda_{k\alpha2}$=1.5444 Å) radiation in the range 2θ = 10 - 70° with a step size of 0.04° and a counting time
240 of 6 seconds per step.

241 *Thermogravimetric analyses:* TGA for all Serpentinized-carbonated samples were performed
242 with a Mettler Toledo TGA/SDTA 851e instrument under the following conditions: sample mass
243 of about 10 mg, 150 µl alumina crucible with a pinhole, heating rate of 10°C min^{-1}, and inert N_2
244 atmosphere of 50 ml min^{-1}. Sample mass loss and associated thermal effects were obtained by
245 TGA/SDTA. In order to identify the different mass loss steps, the TGA first derivative (rate of
246 mass loss) was used. The TGA apparatus was calibrated in terms of temperature. The melting
247 points of three compounds (indium, aluminum and copper) obtained from the DTA signals were
248 used for the sample temperature calibration.

249 *FTIR measurements*: Infrared measurements (in transmission mode) were performed using an IR
250 microscope Bruker Hyperion 3000. The IR beam was focused through a 15x lens and the typical
251 size of infrared spot is 50x50 mm^2. The light source is a Globar (TM) and the beam splitter is in
252 KBr. The spectra were measured from 700 to 4000 cm^{-1} (4 cm^{-1} resolution) with a MCT
253 monodetector cooled by liquid nitrogen. Samples must be thin (less than 100 µm) and flat to
254 avoid absorption band saturation or scattering effects. Sample preparation has involved a careful
255 crushing of samples in mortar and manual compaction of fine crushed particles between two KBr
256 windows. In general, five spectra per sample were collected in different zones and/or aggregates
257 in order to verify their homogeneity/discrepancy.
258

259 **3. Results**

260 3.1. Mineral composition of products

261 The conventional analytic techniques (XRD, TGA, FTIR and FESEM) have revealed that the
262 hydrothermal alteration of olivine using high-carbonate alkalinity solutions, i.e. enriched with

CO_2 (*S1* and *S2 solutions*), concerns the competitive formation of magnesite and serpentine, in other words, competitive carbonation and serpentinization processes during olivine alteration was clearly observed. As expected, both solutions (*S1* and *S2*) have revealed a very similar effect on the olivine alteration because the mineral composition of products and alteration extent were not significantly affected for comparable samples. For specific details, refer to mineral composition evolution summarized in Table 2 for runs 1 to 5 and 16 to 20. Herein, magnesite was observed from 3 days of reaction until the end of experiment (60 days). Conversely, the formation of serpentine (preferentially lizardite type) was retarded with respect to magnesite because it was clearly identified by X-ray diffraction after 10 days of reaction. Chrysotile tubes were also observed by FESEM, preferentially after 30 days reaction. All these qualitative results are summarized in the Figure 1, displaying some XRD patterns and some FESEM images for collected products as the function of reaction time. We note that the experimental duration of 60 days were not enough to transform the available olivine completely into magnesite and serpentine as qualitatively determined by x-ray diffraction (see XRD pattern after 60 days in Figure 1) and by infrared spectroscopy (Fig. 2). This latter analytical tool has confirmed a preferential formation of lizardite polymorph as attested by their two typical stretching infrared modes at 966 and 1085 cm^{-1} for Si-O group (see Fig. 2b). These infrared features are clearly different to infrared features of chrysotile polymorph (Fig. 2c). We remark also that infrared features are in agreement with FESEM observations, which reveal fine particles with platy morphology for lizardite (Fig. 1c) and typical tubular morphology for chrysotile (Fig. 1d). In an effort to quantify "with high-accuracy" the co-formed amount of magnesite and serpentine as a function of time, the thermogravimetric analysis (TGA) were performed at a specific heating rate of 10°C/min under 100% N_2 atmosphere (see materials and methods section for more specific details). Herein,

286 the first derivative curve (DTG) was successfully used to delimit the magnesite and serpentine
287 contents for each reaction-time sample as illustrated in Figure 3. All calculated relative-values for
288 magnesite and serpentine are summarized in Table 1 and they were also used to determine the
289 competitive serpentinization and carbonation rates reported in the sub-section 4.2.
290 Complementary experiments using a serpentinized olivine as starting material (runs 11 to 15), i.e.
291 a mineral material containing chrysotile+brucite+small amount of residual olivine (after Lafay et
292 al., 2012), have revealed a fast carbonation of existing brucite, leading to magnesite formation
293 (see Figure 4). Conversely, insignificant structural effect was measured/observed for interacting
294 chrysotile by using XRD, IR and FESEM. This was experimentally confirmed by using high-
295 purity chrysotile as starting material in other specific experiments (runs 6 to 10) at the same
296 hydrothermal conditions as qualitatively measured by infrared spectroscopy (Figure 5). This solid
297 characterization suggests that chrysotile remains close to equilibrium with respect to interacting
298 solution at the investigated conditions.
299
300 **4. Discussion**
301 4.1. Reaction steps
302 In a previous recent study, we reported that the serpentinization of San Carlos olivine
303 under high-hydroxyl alkalinity "or high-basic conditions" (pH=13.5 ex-situ measured at 20°C)
304 takes place via mineral replacement of olivine by chrysotile and brucite assemblage, i.e. a spatial
305 and temporal coupling of dissolution and precipitation reactions at the interface between olivine
306 and chrysotile–brucite minerals, leading to preservation of external shape of olivine grains
307 (Figure 6a). For more specific details refer to Lafay et al. 2012. Conversely, in the present study
308 using the same pressure-temperature conditions, but, using now CO_2-rich alkaline solutions (*S1*

309 *and S2*) “or high-carbonate alkalinity”, the above mineral replacement reactions has not taken
310 place. In other terms, the original external shape of olivine grains was not preserved as observed
311 by FESEM observations (see for ex. Figure 6d). These observations suggest that the super-
312 saturation for precipitating minerals (magnesite, lizardite and chrysotile) is also reached into the
313 bulk interacting solution, leading to the precipitation of single magnesite crystals and fine
314 particles of serpentine from solution, i.e. that the mineral dissolution was temporally and spatially
315 decoupled of precipitation reactions. However, the nucleation and epitaxial growth processes at
316 the olivine-fluid interfaces cannot be excluded in our investigated system. As mentioned above,
317 competitive precipitation of magnesite and serpentine were clearly determined on solid products;
318 for more simplicity, i.e. excluding the fate of the iron initially contained in olivine, the alteration
319 reaction for olivine under high-carbonate alkalinity can be expressed as follows:

320 $$2Mg_2SiO_4 + 2H_2O + HCO_3^- \rightarrow MgCO_3 + Mg_3Si_2O_5(OH)_4 + OH^- \quad (2)$$

321 This reaction mechanism implied a dissolution process, releasing Mg and Si ions into solution
322 until supersaturation of solution with respect to magnesite and/or serpentine. Their kinetic
323 behavior depends directly on the fluid chemistry such as gradual consumption of dissolved
324 carbonate species and in-situ OH^- regeneration in this closed system. This change of fluid
325 chemistry can probably promote the chrysotile formation at the end of the experiment as
326 observed on FESEM images (Figure 1 (d)). This is possibly due to a decrease of carbonate
327 alkalinity (consumption of HCO_3^-) which is directly proportional to an increase of hydroxyl
328 alkalinity as illustrated in reaction (2). Moreover, recently Lafay et al. (2012) has reported that
329 chrysotile formation is favored under high-hydroxyl alkalinity.
330 On the other hand, the released iron contained in the olivine has not implied any precipitation of

iron oxides or (oxy)hydroxides for runs 1 to 5 and 16 to 20; in fact, the released iron was partially oxidized (about 50%) via a simple reduction of water ($2Fe^{2+} + 2H_2O \rightarrow 2Fe^{3+} + H_2 + 2OH^-$). In this way, the released iron was incorporated in serpentine (as Fe(II) and Fe(III)) and in magnesite (as Fe(II) only). This latter is clearly determined by FESEM/EDS chemical analysis on the single magnesite crystals (Figure 7 concerning run 5).

4.2. Kinetics

The kinetic pseudo-first-order and pseudo-second-order models have been widely used to describe several physicochemical reactions at solid-fluid interfaces such as uptake processes of ions and molecules, photocatalytic oxidation of organic molecules, sorption of vapour water in/on clays, osmotic swelling process of clays, aqueous carbonation of alkaline minerals and crystal growth processes (e.g. Ho and Mckey, 1999; Montes-H and Geraud, 2004; Montes-H, 2005; Ho, 2006; Montes-Hernandez et al., 2009; Montes-Hernandez et al., 2010b). In the present study, the kinetic pseudo-second-order model was specifically used to describe the kinetic behaviour of olivine alteration under hydrothermal conditions (reaction 2) by using the variation of formed mineral(s) content or the alteration extent ξ_{extent} (%) with time t (day). As mentioned above, temporal variation of magnesite and serpentine concerning the reaction (2) was directly determined by using thermogravimetric measurements (see Fig. 3 and Table 1). These kinetic data were successfully fitted using a kinetic pseudo-second-order model. This simple model predicts a fast mass transfer followed by a slow equilibration of mass transfer in closed systems. The differential form for this kinetic model can be written as follows:

$$\frac{d\xi_{extent}}{dt} = k_{alteration}(\xi_{extent,max} - \xi_{extent})^2 \quad (3)$$

where $k_{alteration}$ is the rate constant of olivine alteration [1/% day], $\xi_{extent,max}$ is the maximum value of formed mineral(s) content or alteration extent at apparent equilibrium [%] and ξ_{extent} is the formed mineral(s) content or alteration extent [%] at any time t [day].

The integrated form of Equation (3) for the boundary conditions $t = 0$ to $t = t$ and $\xi_{extent} = 0$ to $\xi_{extent} = \xi_{extent}$, is represented by a hyperbolic relationship:

$$\xi_{extent} = \frac{\xi_{extent,max} * t}{\left(\frac{1}{k_{alteration} * \xi_{extent,max}}\right) + t} \quad (4)$$

Note that the rate constant $k_{alteration}$ (1/% day) has no physical interpretation. For this reason a new parameter can be defined "$(1/k_{alteration} * \xi_{extent,max}) = t_{1/2}$", which represents the duration after which half of the maximum of alteration extent was obtained. The Equation 4 can be then expressed as follows:

$$\xi_{extent} = \frac{\xi_{extent,\max} t}{t_{1/2} + t} \quad (5)$$

In the current study, $t_{1/2}$ is called "half-extent time" and can be used to calculate the initial-rate of olivine alteration, v_0 [1/day] by using the following expression:

$$v_0 = \frac{\xi_{extent,max}}{100 * t_{1/2}} \quad (6)$$

Graphically, the initial rate of olivine alteration v_0 is defined as the slope of the tangent line when the time t tends towards zero on the *r vs. t* curve (see for ex. Montes-Hernandez et al., 2009).

A non-linear regression by the least-squares method was performed to determine these two kinetic parameters ($\xi_{extent,max}$ and $t_{1/2}$) from Eq. 5. All values, including correlation factors and initial alteration rates v_0 are summarized in Table 2. We note that the alteration rates were

372 normalized with respect to initial specific surface area for olivine fine-grains (2.3 m^2/g) deduced
373 from N_2 adsorption isotherm and applying the conventional Brunauer–Emmett–Teller **(**BET)
374 equation.
375 Competitive carbonation (or magnesite formation) and serpentinization (or serpentine formation)
376 concerned in the reaction (2) and displayed in Figure 8 confirm a retarding process of serpentine
377 formation with respect to magnesite (about three times slower); in fact, the magnesite seems to
378 reach an apparent stabilization after about 20 days of reaction while the serpentine follows a
379 progressive slower evolution. We assumed that the magnesite reaches a fast apparent equilibrium
380 with solution because the available carbonate species are not renewed from gas phase as typically
381 constrained in aqueous carbonation experiments where a given CO_2 pressure is imposed in the
382 system (e.g. Bearat et al., 2006). In this way, the serpentinization process remains active until the
383 end of experiment and the carbonation process seems to be inhibited after about 30 days in the
384 system as shown in Figure 8. On the other hand, the alteration rate of olivine in presence of
385 dissolved CO_2 or under high-carbonate alkalinity (1.8636×10^{-9} mol/m^2 s) is significantly retarded
386 with respect to a CO_2-free system or under high-hydroxyl alkalinity at the same P-T-grain size-
387 solid/fluid ratio conditions (1.6659×10^{-8} mol/m^2 s) as illustrated in Figure 9. As invoked above,
388 the chrysotile and brucite were preferentially formed under high-hydroxyl alkalinity and the
389 original external shape of olivine grains was preserved (Lafay et al., 2012). Conversely, under
390 high-carbonate alkalinity, lizardite and magnesite were preferentially formed and the original
391 external shape of olivine grains was not preserved (Figure 6d).
392
393
394

395 4.3. Role of pH and fluid chemistry

396 In a previous recent study, we demonstrated that high-hydroxyl alkalinity (1M NaOH, pH=13.5
397 at 20°C) promote a fast serpentinization process of San Carlos olivine (Lafay et al., 2012), if it is
398 compared with experimental serpentinization of olivine in high-purity water or in salt solution
399 (seawater analogue) already reported by Malvoisin et al. (2012). This latter study has clearly
400 described the influence of temperature and initial grain size on the serpentinization rate. In
401 general, the serpentinization rate increases with a decrease of initial grain size and an increase of
402 temperature from 200 to 350°C (Malvoisin et al., 2012). However, the serpentinization rate of
403 olivine can also depend on the fluid/solid ratio, fluid hydrodynamics and fluid chemistry
404 (including pH) as suggested by field fluid monitoring and modeling studies (e.g Charlou et al.,
405 2002; Früh-Green et al., 2003; Allen et al., 2004; Ludwig et al., 2006; Seyfried et al., 2011). In
406 this way, the present study has revealed that a simple change in alkalinity from high-hydroxyl
407 alkalinity (1M NaOH, pH=13.5 at 20°C) to high-carbonate alkalinity (1M $NaHCO_3$, pH=8.9 at
408 20°C) retards significantly the alteration process of olivine (Figure 9), leading to a preferential
409 formation of lizardite and magnesite. Moreover, the spatial and temporal coupling of dissolution
410 and precipitation reactions (or mineral replacement reactions) was not observed under high-
411 carbonate alkalinity. This means that the fluid chemistry and pH play an important role on the
412 alteration kinetics, reaction mechanisms and nature of solid-gas products during olivine alteration
413 in natural hydrothermal systems. The effect of pH on the dissolution rate of olivine and/or of
414 forsteritic olivine has been assessed using continuous, semi-continuous or discontinuous
415 experimental systems (e.g. Pokrovsky and Schott, 2000; Rosso and Rimstidt, 2000; Chen and
416 Brantley, 2000; Hänchen et al., 2006; Daval et al., 2011). However, the effect of pH on the

serpentinization rate for olivine is more difficult to be experimentally assessed because it implies dissolution of primary components followed by precipitation of secondary mineral phases and H_2 production whether redox reactions are significant (e.g. Marcaillou et al., 2011; Malvoisin et al., 2012; Lafay et al., 2012). In an effort, to evaluate the pH effect on the serpentinization rate, the olivine serpentinization was recently investigated under high-hydroxyl alkalinity (pH=13.5 at 20°C) (Lafay et al., 2013). This extreme scenario has provided interesting insights on the kinetics and reaction mechanism. For example, the magnetite (Fe_3O_4) secondary mineral phase, typically observed from olivine serpentinization in high-purity water at T>200°C (Marcaillou et al. 2011 and Malvoisin et al., 2012) was not observed under high-hydroxyl alkalinity. However, the magnetite formation during serpentinization is frequently related to redox reactions and/or H_2 production (McCollom and Bach, 2009; Marcaillou et al., 2011); herein, we note that the H_2 production is not necessary associated to magnetite precipitation because it can be produced by simple oxidation of Fe(II) (initially contained in olivine) followed by a simple reduction of water as expressed by the following coupled oxidation-reduction reaction ($2Fe^{2+} + 2H_2O \rightarrow 2Fe^{3+} + H_2 + 2OH^-$). In fact, the oxidized iron (Fe(III)) and reduced iron (Fe(II)) can be selectively incorporated and/or sequestered in major secondary phases (serpentine, brucite, magnesite..) (e.g. Klein et al., 2009; Lafay et al., 2012; this study); this limits the formation of iron oxides and/or oxyhydroxides in specific environments. Under high alkalinity, preliminary Mössbauer spectroscopy measurements (results not shown here) on two selected samples have revealed a partial iron oxidation (≈50%) from Fe(II) to Fe(III) of initial iron contained in olivine. Moreover, FESEM//EDS chemical analyses have revealed that single crystals of magnesite contain significant amount of iron. We note that only Fe(II) can be incorporated into magnesite crystals; this confirms also a partial oxidation. Based on this result, the H_2 production is expected in our

system and could be roughly quantified, but, this specific study was mainly oriented on the simultaneous serpentinization and aqueous carbonation of olivine.

On the other hand, some serpentinization experiments (runs 21 to 24 in Table 1) under high-acidic solutions (initial pH=0.66) have revealed slower serpentinization rates and a more complex kinetic behavior (sigmoidal kinetic behavior: $[\xi_{extent} = \xi_{extent,\max}/(1+\exp(-(t-t_{1/2})/b))]$) than under high-hydroxyl alkalinity (Lafay et al., 2012) and under high-carbonate alkalinity (this study); however, as expected, the pH increases proportionally with serpertinization progress (see Figure 10), because by definition the dissolution of olivine (ultrabasic rock) in acidic solutions and in discontinuous (or closed) systems, implies a transient consumption of protons (H^+) and the production of hydroxyl ions (OH^-) until the solution supersaturation with respect to serpentine, brucite and other minor mineral phases (e.g. TOT clays and iron oxides/oxyhydroxides),. The brucite mineral ($Mg(OH)_2$) is a direct proof of hydroxyl ion production in the system. A simplified reaction mechanism for serpentinization of olivine in acidic solution and in batch system, i.e. excluding the fate of initial Fe(II) contained in olivine, can be expressed as follows:

Dissolution step,

$$2Mg_2SiO_4 + 4H_2O + 4H^+ \rightarrow 4Mg^{2+} + 2H_4SiO_{4(aq)} + 4OH^- \quad (7a)$$

Precipitation from solution and/or nucleation-growth processes at olivine-fluid interfaces,

$$4Mg^{2+} + 2H_4SiO_{4(aq)} + 4OH^- \rightarrow Mg_3Si_2O_5(OH)_4 + Mg(OH)_2 + H_2O + 4H^+ \quad (7b)$$

The summation of these two reaction steps (7a) and 7(b) gives a classic serpentinization global reaction for forsteritic olivine as described in many previous studies:

460 $$2Mg_2SiO_4 + 3H_2O \rightarrow Mg_3Si_2O_5(OH)_4 + Mg(OH)_2 \quad (7c)$$

461 This global serpentinization reaction for San Carlos olivine, initiated at low pH (=0.66), is in
462 agreement with thermogravimetric measurements reported in Table 1 (runs 21 to 24) and in
463 Figure 10. However, we note that minor other mineral phases were also identified from XRD
464 patterns in these experiments such as the hydro-hematite and TOT clay (talc type).

465

466 4.4 Is "silica passivating layer" a universal process during olivine alteration?

467 The formation of passivating layers during solid-fluid interfacial processes are widely
468 documented in materials sciences and chemical engineering areas. For example, in gas-solid
469 carbonation of alkaline sorbents, the CO_2-sorbent reaction typically takes place by the formation
470 of a dense non-porous layer of carbonate (or protective carbonate layer) around the reacting
471 particles. For these cases, the carbonation reaction is generally stopped before a complete
472 carbonation (e.g., Fernandez Bertos et al., 2004; Sun et al., 2008; Prigiobbe et al., 2009;
473 Stendardo and Foscolo, 2009; Huntzinger et al., 2009). Conversely, recent studies have
474 demonstrated that the formation of a so-called passivating layer of carbonate depend strongly on
475 the intrinsic textural properties of reacting particles and on the experimental conditions such as
476 relative humidity, CO_2 pressure, fluid dynamics and temperature (e.g. Beruto and Botter, 2000;
477 Dheilly et al., 2002; Seo et al., 2007; Zeman, 2008; Montes-Hernandez et al. 2010a and 2010b;
478 Montes-Hernandez et al., 2012). In this way, the formation of a protective carbonate layer leads
479 to a physical increase in volume at the grain scale (expansion or swelling process) or a decrease
480 in porosity (pore closure process) when porous materials are partially carbonated (Fernandez

Bertos et al., 2004; Chen et al., 2007; Sun et al., 2008). Concerning the olivine aqueous alteration under acid conditions or under high CO_2 pressure (>20bar), incongruent dissolution process has been measured, leading to a Si-rich layer alteration profile around reacting olivine grains (e.g. Wogelius and Walther, 1991; Pokrovsky and Schott, 2000; Rosso and Rimstidt, 2000; Prigiobbe et al., 2009); its progressive formation generally leads to a passivating effect "limiting reaction process". Similar to gas-solid carbonation process, the formation of a silica layer around the olivine reacting particles could passivate or squarely stopper the interfacial reaction as already invoked by Daval et al., 2011. However, the mechanistic pathway of its formation is still debated in the literature; some authors have proposed a polymerization process via an ion-exchange reaction ($Mg^{2+} \leftrightarrow 2H^{+}$) and formation of surface ($\equiv Si(OH)_4$) monomers that polymerize to a porous or non-porous silica layer (e.g. Wogelius and Walther, 1991; Chen and Brantley, 2000; Pokrovsky and Schott, 2000; Béarat et al., 2006). Conversely, other recent studies have proposed a temporal and spatial coupling of Si release ($H_4SiO_{4(aq)}$) and silica precipitation process ($SiO_{2(s)}$ layer) (e.g. Daval et al., 2011), initially proposed by Hellmann et al. (2003) for labradorite feldspar altered under acid pH. This implies that the silica phase reaches a rapid supersaturation near of the reacting mineral phase. In this context and based on our recent results (Lafay et al., 2012 and this study), we assume that a silica passivating layer during alteration of olivine is only formed under high acid conditions (pH<4), including high CO_2 pressure (>20 bar) because under high hydroxyl or carbonate alkalinity conditions (9<pH≤13.5), the formation of so-called silica passivating layer was not determined/suspected by XRD, FTIR and TGA measurements. This observation is in agreement with a previous study and explanations provided by Pokrovsky and Schott, (2000).

5. Coexistence of carbonation and serpentinization processes: from experimentation to natural systems

In the last decades, the serpentinization of olivine have been intensively investigated at the lab scale in order to determine the reaction mechanisms and kinetics, the reaction and cracking propagation from the grain boundaries, its potential for hydrogen production and its implications on the early Earth life, i.e. its role on the abiotic formation of organic molecules (MacLeod et al., 1994; James et al., 3003; McCollom and Bach, 2009; Seyfried et al., 2007; Hövelmann et al., 2011; Marcaillou et al., 2011; Malvoisin et al., 2012; Lafay et al., 2012). Obviously, these studies have direct relevance in Earth systems, but, they are systematically oriented to investigate the olivine alteration in high-purity water, in saline water (seawater analogue) or in acidic solutions. In this way, we demonstrated that the olivine alteration under high alkalinity conditions follows different reaction mechanisms and the kinetic behaviour is drastically modified as explained above. On the other hand, direct and indirect aqueous carbonation of olivine is intensively being investigated in order to determine the best experimental conditions for ex-situ mineral sequestration of CO_2 using natural olivine. Herein, the Albany Research Centre has reported that the optimum sequestration reaction conditions observed to date are 1M NaCl + 0.64M $NaHCO_3$ at T≈180°C and P_{CO2}≈135 bar (Chen et al., 2006; Béarat et al., 2006; King et al, 2010;Daval et al., 2011). In this context, Béarat et al. (2006) have concluded that mitigating passivating layer effectiveness is critical to enhancing carbonation and lowering sequestration process cost. Inspired on these independent results of olivine serpentinization and aqueous carbonation, specific novel experimental conditions were used in this study (1M $NaHCO_3$ solution, pH ≈ 9, 200°C and saturated vapor pressure) in order to investigate a competitive effect between

525 serpentinization and aqueous carbonation of olivine. These simple experimental constraints could
526 contribute to a better understanding of fluid-rock interactions in natural active hydrothermal
527 Earth fields such as Samail Ophiolite in Oman, New Caledonia Ophiolite, etc. where a
528 simultaneous serpentinization and aqueous carbonation processes are currently expected (e.g.
529 Kelemen and Matter, 2008; Matter and Kelemen, 2009).

530 **6. Implications for in-situ carbonation of peridotite for CO_2 storage**

531 Unregulated CO_2 emissions into the Earth's atmosphere (about $22x10^9$ ton CO_2/year), caused
532 mainly by fossil fuel combustion, have led to concerns about global warming. To maintain the
533 atmospheric CO_2 level below 500 ppm, CO_2 emissions will have to be stabilized at current levels,
534 although they are forecast to double over the next 50 years (Allwood et al., 2010). Capture from
535 individual industrial sources and long-term geological storage are realistic and available ways of
536 reducing CO_2 emissions because large volumes of this gas can be stored in various deep
537 geological formations (e.g. Knauss et al., 2005; Friedmann, 2007; IPCC, 2007; Bachu, 2008).
538 Recently, Kelemen and Matter (2008) have proposed the in-situ carbonation of peridotite for CO_2
539 storage, i.e. the injection of purified CO_2 in peridotite massifs. This conceptual methodology
540 requires obviously drilling, hydraulic fracturing, the use of $NaHCO_3$ as catalyst, pumping fluid
541 and preheating fluid for the first heating step. In this way, the authors have estimated very fast
542 carbonation of peridotite compared with natural peridotite hydration and carbonation in the
543 Samail Ophilite (Oman) and have reported that the in-situ carbonation of peridotite could
544 consume >1 billion tons of CO_2 per year in Oman alone. In this context, the basic research in the
545 coming years on the simultaneous hydration (and/or serpentinization) and carbonation rates of
546 peridotite "from strategic fields" could have relevant implications for this promising potential

547 alternative for CO_2 storage. In addition, sophisticated experimental setups could be designed to
548 evaluate hydraulic fracturing and reactive percolation in fractured-porous media under high
549 confinement pressure and temperature in order to evaluate the swelling process and associated
550 micro-fracturing related to hydration and/or carbonation processes of peridotite. Technically, this
551 is feasible because various percolation experiments simulating the reactivity of supercritical CO_2
552 have already been reported (e.g. Le Guen et al., 2007; Andreani et al., 2009).

553

554 **7. Conclusion**

555 The coexistence of serpentinization and aqueous carbonation of ultrabasic rocks has up to now
556 not been investigated at laboratory scale and various questions still remain unanswered
557 concerning its mechanistic pathways in natural systems, mainly under high alkalinity. In response
558 to this scientific gap, this study provides new insights on competitive serpentinization and
559 aqueous carbonation of olivine under high-carbonate alkalinity. In this way, we quantified a
560 retarding process of serpentine formation with respect to magnesite (about three times slower) by
561 using a simple kinetic pseudo-second-order model; in fact, the magnesite seems to reach an
562 apparent stabilization after about 20 days of reaction while the serpentine follows a progressive
563 slower evolution. We assumed that the magnesite has reached a fast apparent equilibrium with
564 solution because the available carbonate species are not renewed from fluid phase as typically
565 constrained in aqueous carbonation experiments where a given CO_2 pressure is imposed in the
566 system. In summary, we demonstrated that a simple change of fluid chemistry (including pH) has
567 a significant impact on the reaction mechanism and kinetics for olivine alteration at a given
568 temperature. Some FESEM/EDS chemical analyses and preliminary Mössbauer measurements

have revealed that about 50% of initial Fe(II) was oxidized to Fe(III). The not oxidized iron in solution (Fe(II)) from reacting olivine was preferentially incorporated into magnesite crystals. This means a classic hydrogen production via a simple water reduction. The full quantification of redox reactions during simultaneous serpentinization and carbonation of olivine and peridotite under high carbonate alkalinity remains a future challenge.

Acknowledgements

The authors are grateful to the French National Center for Scientific Research (CNRS/INSU), the University Joseph Fourier in Grenoble and ANR French research agency (ANR CORO and ANR SPRING projects) for providing financial support.

614 **References**

615 Allen D. E., Seyfried W. E. Jr. (2004) Sepentinization and heat generation: constraints from Lost
616 City and Rainbow hydrothermal systems. *Geochim. Cosmochim. Acta* **68**, 1347-1354.

617 Andreani M., Luquot L., Gouze P., Godard M., Hoisé E., Gibert B. (2009) Experimental study of
618 carbon sequestration reactions controlled by the percolation of CO_2-rich brine through
619 peridotites. *Environ. Sci. Technol.* **43**, 1226-1231.

620 Bachu S. (2000) Sequestration of CO_2 in geological media: criteria and approach for site
621 selection in response to climate change. *Energy Convers. Manage.* **41**, 953-970.

622 Bachu S. (2008) CO_2 storage in geological media: role, means, status, barriers to deployment.
623 *Prog. Energy Combust. Sci.* **34**, 254-273.

624 Bearat H., Mckelvy M. J., Chizmeshya A. V. G., Gormley D., Nunez R., Carpenter R. W.,
625 Squires K., Wolf G. H. (2006) Carbon sequestration via aqueous olivine mineral carbonation:
626 Role of passivating layer formation. *Environ. Sci. Technol.* **40**, 4802-4808.

627 Beruto D. T., Botter R., (2000) Liquid-like H_2O adsorption layers to catalyse the $Ca(OH)_2/CO_2$
628 solid-gas reaction and to form a non-protective solid product layer at 20°C. *J. European*
629 *Ceramic Soc.* **20**, 497-503.

630 Bonfils B., Julcour-Lebigue C., Guyot F., Bodénan F., Chiquet P., Bougeois F. (2012)
631 Comprehensive analysis of direct aqueous mineral carbonation using dissolution enhancing
632 organic additives. *Int. J. Greenhouse Gas Control* **9**, 334-346.

633 Charlou J. L., Donval J. P., Fouquet Y., Jean-Baptiste P., Holm N. (2002) Geochemistry of high

H_2 and CH_4 vent fluids issuing from ultramafic rocks at the Rainbow hydrothermal field (36° 14'N, MAR). *Chem. Geol.* **191**, 345-359.

Chen M., Wang N., Yu J., Yamaguchi A. (2007) Effects of porosity on carbonation and hydration resistance of CaO materials. *J. European Ceram. Soc.* **27**, 1953-1959.

Chen Y., Brantley S. L. (2000) Dissolution of forsteritic olivine at 65°C and 2<pH<5. *Chem. Geol.* **165**, 267-281.

Chen Z.-Y., O'Connor W. K., Gerdemann S. J. (2006) Chemistry of aqueous mineral carbonation for carbon sequestration and explanation of experimental results. *Environ. Progress* **25**, 161-166.

Daval D., Sissmann O., Menguy N., Saldi G. D., Guyot F., Martinez I., Corvisier J., Garcia B., Machouk I., Knauss K. G., Hellmann R. (2011) Influence of amorphous silica layer formation on the dissolution rate of olivine at 90°C and elevated pCO_2. *Chem. Geol.* **284**, 193-209.

Dheilly R. M., Tudo J., Sebai Y., Queneudec M. (2002) Influence of storage conditions on the carbonation of powdered $Ca(OH)_2$. *Construction and Building Materials* **16**, 155-161.

Fernandez Bertos M., Simons S. J. R., Hills C. D., Carey P. J. (2004) A review of accelerated carbonation technology in the treatment of cement-based materials and sequestration. *J. Hazard. Mater.* **B112**, 193-205.

Friedmann S. J. (2007) Geological carbon dioxide sequestration. *Elements* **3**, 179-184

Fritz B., Clément A., Montes-Hernandez G., Noguera, C. (2013) Calcite formation by hydrothermal carbonation of portlandite : Complementary insights from experiment and

654 simulation. *CrystEngComm* **15**, 3392-3401.

655 Früh-Green G. L., Kelley D. S., Bernasconi S. M., Karson J. A., Ludwig K. A., Butterfield D. A.,
656 Boschi C., Proskurowski G. (2003) 30,000 years of hydrothermal activity at the Lost City vent
657 field. *Science* **301**, 495-498.

658 Garcia B., Beaumont V., Perfetti E., Rouchon V., Blanchet D., Oger P., Dromart G., Huc A.-Y.,
659 Haeseler F. (2010) Experiments and geochemical modeling of CO_2 sequestration by olivine:
660 Potential, quantification. *Appl. Geochem.* **25**, 1383-1396.

661 Gerdemann S. J., O'Connor W. K., Dahlin D. C., Penner L. R., Rush H. (2007) Ex situ aqueous
662 mineral carbonation. *Environ. Sci. Technol.* **41**, 2587-2593.

663 Giammar D. E., Bruant R. G., Peters A. (2005) Forsterite dissolution and magnesite precipitation
664 at conditions relevant for deep saline aquifer storage and sequestration of carbon dioxide.
665 *Chem. Geol.* **217**, 257-276.

666 Hänchen M., Prigiobbe V., Storti G., Seward T. M., Mazzotti M. (2006) Dissolution kinetics of
667 forsteritic olivine at 90-150°C including effects of the presence of CO_2. *Geochim. Cosmochim.*
668 *Acta* **70**, 4403-4416.

669 Hellmann R., Penisson, J.-M., Hervig R. L., Thomassin, J.-H., Abrioux M.-H. (2003) An
670 EFTEM/HRTEM high-resolution study of the near surface of labradorite feldspar altered at
671 acid pH: evidence for interfacial dissolution-reprecipitation. *Phys. Chem. Minerals* **30**, 192-
672 197.

673 Ho Y-S., McKay G. (1999) Pseudo-second order model for sorption processes. *Proc. Biochem.*

674 **34**, 451-465.

675 Ho Y-S. (2006) Review of second-order models for adsorption systems. *J. Hazard. Mater*. **B136**,
676 681-689.

677 Hövelmann J., Austrheim H., Beinlich A., Munz I. A. (2011) Experimental study of the
678 carbonation of partially serpentinized and weathered peridotites. *Geochim. Cosmochim. Acta*
679 **75**, 6760-6779.

680 Huntzinger D. N ., Gierke J. S., Kawatra S. K., Eisele T. C., Sutter L. L. (2009) Carbon dioxide
681 sequestration in cement kiln dust through mineral carbonation. *Environ. Sci. Technol.* **43**,
682 1986-1992.

683 IPCC (Intergovernmental Panel on Climate Change), Climate Change **2007**: Climate Change
684 Impacts, Adaptations and Vulnerability, 2007.

685 James R. H., Allen D. E., Seyfried W. E. Jr. (2003) An experimental study of alteration of
686 oceanic crust and terrigenous sediments at moderate temperatures (51 to 350°C): Insights as to
687 chemical processes in near-shore ridge-flank hydrothermal systems. *Geochim. Cosmochim.*
688 *Acta* **67**, 681-691.

689 Kaszuba J. P., Janecky D. R., Snow M. G. (2003) Carbon dioxide reaction processes in a model
690 brine aquifer at 200°C and 200 bars: Implications for geologic sequestration of carbon. *Appl.*
691 *Geochem.* **18**, 1065-1080.

692 Kaszuba J. P., Janecky D. R., Snow M. G. (2005) Experimental evaluation of mixed fluid
693 reactions between supercritical carbon dioxide and NaCl brine: Relevance to the integrity of a

694 geologic carbon repository. *Chem. Geol.* **217**, 277-293.

695 Kelemen P. B., Matter J. M. (2008) In situ carbonation of peridotite for CO_2 storage. *Proc. Natl.*
696 *Acad. Sci. USA* **105**, 17295-17300.

697 Kelemen P. B., Matter J. M., Streit E. E., Rudge J. F., Curry W. B., Blusztajn J. (2011) Rates and
698 mechanisms of mineral carbonation in peridotite: Natural processes and recipes for enhanced,
699 in situ CO_2 capture and storage. *Annu. Rev. Earth Planet. Sci.* **39**, 545-576.

700 Kelley D. S., Karson J. A., Blackman D. K., Früh-Green, G. L. *et al.* (2001) An off-axis
701 hydrothermal vent field near the Mid-Atlantic Ridge at 30° N. *Nature* **412**, 145-149.

702 Kelley D. S., Karson J. A., Früh-Green, G. L., Yoerger D. R., *et al.* (2005) A Serpentinite-Hosted
703 Ecosystem: The Lost City Hydrothermal Field. *Science* **307**, 1428-1434.

704 King H. E., Plümper O., Putnis A. (2010) Effect of secondary phase formation on the carbonation
705 of olivine. *Environ. Sci. Technol.* **44**, 6503-6509.

706 Klein F., Bach W., Jöns N., McCollomb T., Moskowitz B., Berquó T. (2009) Iron partitioning
707 and hydrogen generation during serpentinization of abyssal peridotites from 15°N on the Mid-
708 Atlantic Ridge. *Geochim. Cosmochim. Acta* **73**, 6868-6893.

709 Klein F., Garrido C. J. (2011) Thermodynamic constraints on mineral carbonation of
710 serpentinized peridotite. *Lithos* **126**, 126-160.

711 Knauss K. G., Johnson J. W., Steefel C. I. (2005) Evaluation of the impact of CO_2, co-
712 contaminant gas, aqueous fluid and reservoir rock interactions on the geological sequestration
713 of CO_2. *Chem. Geol.* **217**, 339-350.

714 Lackner K. S., Wendt C. H., Butt D. P. Joyce E. I., Sharp D. H. (1995) Carbon dioxide disposal
715 in carbonate minerals. *Energy* **20**, 1153-1170.

716 Lafay R., Montes-Hernandez G., Janots E., Chiriac R., Findling N., Toche F. (2012). Mineral
717 replacement rate of olivine by chrysotile and brucite under hihg alkaline conditions. *J. Cryst.*
718 *Growth* **347**, 62-72.

719 Lafay, R., Montes-Hernandez G., Janots E., Chiriac R., Findling, N., Toche F. (2013) Nucleation
720 and growth of chrysotile nanotubes in H_2SiO_3-$MgCl_2$-NaOH medium from 90 to 300°C.
721 *Chem. Eur. J.* **19**, 5417-5424.

722 Le Guen Y., Renard F., Hellmann R., Collombet M., Tisserand D., Brosse E., and Gratier J.-P.
723 (2007) Enhanced deformation of limestone and sandstone in the presence of a high pCO2
724 fluids. *J. Geophys. Res.* **112**, B05421, doi:10.1029/2006JB004637.

725 Ludwig K. A., Kelley, D. S., Butterfield D. A., Nelson B. K., Früh-Green G. (2006) Formation
726 and evolution of carbonate chimneys at the Lost City hydrothermal field. *Geochim.*
727 *Cosmochim. Acta* **70**, 3625-3645.

728 MacLeod G., McKeown C., Hall A. J., Russell M. J. (1994) Hydrothermal and oceanic pH
729 conditions of possible relevance to the origin of life. *Orig. Life Evol. Biosph.* **23**, 19-41.

730 Malvoisin B., Brunet F., Carlut J., Rouméjon S., Cannat M. (2012) Serpentinization of oceanic
731 peridotites : 2. Kinetics and processes of San Carlos olivine hydrothermal alteration. *J.*
732 *Geophys. Res.* **117**, B04102, doi : 10.1029/2011JB008842.

733 Marcaillou C., Muñoz M., Vidal O., Parra T., Harfouche M. (2011) Mineralogical evidence for

734 H_2 degassing during serpentinization at 300°C/300 bar. *Earth Planet. Sci. Lett.* **303**, 281-290.

735 Matter J. M., Kelemen P. B. (2009) Permanent CO_2 storage and mineral carbonation in geologic
736 reservoirs. *Nat. Geosci.* **2**, 837-841.

737 McCollom T. M., Bach T. M. (2009) Thermodynamic constraints on the hydrogen generation
738 during serpentanization of ultramafic rocks. *Geochim. Cosmochim. Acta* **73**, 856-875.

739 Montes-H G., Geraud Y. (2004) Sorption kinetic of water vapour of MX80 bentonite submitted
740 to different physical-chemical and mechanical conditions. *Colloids and Surfaces A:*
741 *Physicochem. Eng. Aspects* **235,** 17-23.

742 Montes-H G. (2005) Swelling-shrinkage measurements of bentonite by using coupled
743 environmental scanning electron microscopy and digital images analysis. *J. Colloids Interface*
744 *Sci.* **284**, 271-277.

745 Montes-Hernandez G., Fernandez-Martinez A., Renard F. (2009) Novel Method to estimate the
746 linear growth rate of submicrometric calcite produced in a triphasic gas-liquid-solid system.
747 *Cryst. Growth Des.* **9**, 4567-4573.

748 Montes-Hernandez G., Perez-Lopez R., Renard F., Nieto J.-M., Charlet L. (2009) Mineral
749 sequestration of CO_2 by aqueous carbonation of coal combustion fly-ash. *J. Hazard. Mat.* **161**,
750 1347-1354.

751 Montes-Hernandez G., Pommerol A., Renard F., Beck P., Quirico E., Brissaud O. (2010a) In-situ
752 kinetic measurements of gas-solid carbonation of $Ca(OH)_2$ by using an infrared microscope
753 coupled to a reaction cell. *Chem. Eng. J.* **161**, 250-256.

754 Montes-Hernandez G., Daval D., Chiriac R., Renard F. (2010b) Growth of nanosized calcite
755 through gas-solid carbonation of nanosized portlandite particles under anisobaric conditions.
756 *Cryst. Growth Des.* **10**, 4823-4830.

757 Montes-Hernandez G., Renard F., Chiriac R., Findling N., Toche F. (2012) Rapid precipitation of
758 magnesite micro-crystals from $Mg(OH)_2$-H_2O-CO_2 slurry enhanced by NaOH and a heat-
759 ageing step (from ~20 to 90°C). *Cryst. Growth Des.* **12**, 5233-5240.

760 Montes-Hernandez G., Chiriac R., Toche F., Renard F. (2012) Gas-solid carbonation of Ca(OH)2
761 and CaO particles under non-isothermal and isothermal conditions by using a
762 thermogravimetric analyzer : Implications for CO2 capture. *Int. J. Greenhouse Gas Control*
763 **11**, 172-180.

764 Oelkers E. H., Gislason S. R., Matter J. (2008) Mineral carbonation of CO_2. *Elements* **4**, 333-337.

765 Parkhurst D. L., Appelo C. A. J. (1999) Users guide to PHREEQC (version 2) – A computer
766 program for speciation, batc reaction, one dimensional transport and inverse geochemical
767 calculations. U. S Geological Survey Water-Resources investigation report 99-4259, 312pp.

768 Pokrovsky O. S., Schott J. (2000) Kinetics and mechanism of forsterite dissolution at 25°C and
769 pH from 1 to 12. *Geochim. Cosmochim. Acta* **64**, 3313-3325.

770 Prigiobbe V., Polettini A., Baciocchi R. (2009) Gas-solid carbonation kinetics of air pollution
771 control residues for CO_2 storage. *Chem. Eng. J.* **148**, 270-278.

772 Prigiobbe V., Costa, G., Baciocchi R., Hänchen M., Mazzoti M. (2009) The effect of CO_2 and
773 salinity on olivine dissolution kinetics at 120°C. *Chem. Eng. Sci.* **64**, 3510-3515.

774 Paukert A. N., Matter J. M., Kelemen P. B., Shock E. L., Havig J. R. (2012) Reaction path
775 modelling of enhanced in-situ CO_2 mineralization for carbon sequestration in the peridotite of
776 the Samail Ophiolite, Sultanate of Oman. *Chem. Geol*. **330-331**, 86-100.

777 Rosso J. J., Rimstidt D. J. (2000) A high resolution study of forsterite dissolution rates. *Geochim.*
778 *Cosmochim. Acta* **64**, 797-811.

779 Rudge J. F., Kelemen P. B., Spiegelman M. (2010) A simple model of reaction-induced cracking
780 applied to serpentinization and carbonation of peridotite. *Earth Planet. Sci. Lett.* **291**, 215-227.

781 Schrenk M. O., Brazelton W. J., Lang S. Q. (2013) Serpentinization, carbon, and deep life. *Rev.*
782 *Mineral. Geochem.* **75**, 575-606.

783 Schwarzenbach E. M., Früh-Green G. L., Bernosconi S. M., Alt J. G., Plas A. (2013)
784 Serpentinization and carbon sequestration: A study of two ancient peridotite-hosted
785 hydrothermal systems. *Chem. Geol*. **351**, 115-133.

786 Seifritz W. (1990) CO_2 disposal by means of silicates. *Nature* **345**, 486

787 Seo Y., Jo S-H., Ryu C. K., Yi C-K. (2007) Effects of water vapour pretreatment time and
788 reaction temperature on CO_2 capture characteristics of a sodium-based solid sorbent in a
789 bubbling fluidized-bed reactor. *Chemosphere* **69**, 712-718.

790 Seyfried W. E. Jr., Foustoukos D. I., Fu Q. (2007) Redox evolution and mas transfer during
791 serpentinization: An experimental and theoretical study at 200°C, 500 bar with implications
792 for ultramafic-hosted hydrothermal systems at Mid-Ocean Ridges. Geochim. Cosmochim.
793 Acta 71, 3872-3886.

794 Seyfried W. E. Jr., Pester N. J., Ding K., Rough M. (2011) Vent fluid chemistry of the Rainbow
795 hydrothermal system (36°N, MAR): Phase equilibria and in situ pH controls on subseafloor
796 alteration processes. Geochim. Cosmochim. Acta 75, 1574-1593.

797 Stendardo S., Foscolo P. U. (2009) Carbon dioxide capture with dolomite: A model for gas-solid
798 reaction within the grains of a particulate sorbent. *Chem. Eng. Sci.* **64**, 2343-2352.

799 Streit E., Kelemen P., Eiler J. (2012) Coexisting serpentine and quartz from carbonate-bearing
800 serpentinized peridotite in the Samail Ophiolite, Oman. *Contrib. Mineral Petrol.* **164**, 821-
801 837.

802 Sun P., Grace J. R., Lim C. J., Anthony E. J., 2008. A discrete-pore-size-distribution-based gas-
803 solid model and its application to the CaO + CO_2 reaction. *Chem. Eng. Sci.* **63**, 57-70.

804 Wogelius R. A., Walther J. V. (1991) Olivine dissolution at 25°C: effects of pH, CO_2, and
805 organic acids. *Geochim. Cosmochim. Acta* **55**, 943-954.

806 Wunder B., Schreyer W. (1997) Antigorite: high-pressure stability in the system MgO-SiO_2-H_2O
807 (MSH). *Lithos* **41**, 213-227.

808 Xu W. Y., Apps J.A., Pruess K. (2004) Numerical simulation of CO_2 disposal by mineral
809 trapping in deep aquiefers. *Appl. Geochem.* **19**, 917-936.

810 Zeman F. (2008) Effect of steam hydration on performance of lime sorbent for CO_2 capture. *Int.*
811 *J. Greenhouse Gas Control* **2**, 203-209.

812

813 Table 1. Summary of experimental conditions and thermogravimetric analyses (TGA)

Run #	Starting material	Time (days)	Solution	pH		Product amount (%) from TGA			
				initial	final	Serpentine	Magnesite	Brucite	Residual olivine
1	Ol	3	S1	8.9	9.17	4.0	12.8	-	83.2
2	Ol	10	S1	8.9	9.38	21.6	14.9	-	63.5
3	Ol	20	S1	8.9	9.63	18.5	25.5	-	56.0
4	Ol	33	S1	8.9	9.55	27.0	23.7	-	49.3
5	Ol	60	S1	8.9	9.58	40.6	26.6	-	32.8
6	Ctl	3	S1	8.9	9.05	95.4	4.6	-	-
7	Ctl	11	S1	8.9	9.18	95.4	4.6	-	-
8	Ctl	22	S1	8.9	9.25	95.8	4.2	-	-
9	Ctl	32	S1	8.9	9.19	95.7	4.3	-	-
10	Ctl	78	S1	8.9	8.83	96.8	3.2	-	-
11	Ctl+bru	3	S1	8.9	9.57	82.9	17.1	-	-
12	Ctl+bru	10	S1	8.9	9.57	82.6	17.4	-	-
13	Ctl+bru	20	S1	8.9	9.59	83.6	16.4	-	-
14	Ctl+bru	33	S1	8.9	9.58	81.3	18.7	-	-
15	Ctl+bru	60	S1	8.9	9.66	79.0	21.0	-	-
16	Ol	3	S2	8.7	9	2.8	10.1	-	87.0
17	Ol	10	S2	8.7	9.4	19.6	16.6	-	63.8
18	Ol	20	S2	8.7	9.45	26.7	22.8		50.5
19	Ol	23	S2	8.7	9.49	24.8	20.9	-	54.4
20	Ol	60	S2	8.7	9.57	46.7	23.0	-	30.3
21	Ol	10	S3	0.63	4.77	3.8	-	<1	96.2
22	Ol	66	S3	0.63	6.37	14.5	-	<1	85.5
23	Ol	90	S3	0.63	7.29	33.1	-	5	62.9
24	Ol	183	S3	0.63	7.95	71.4	-	7.9	20.7

814 All experiments were carried out at 200°C and saturated vapor pressure. Fluid/solid weight ratio
815 is always ≈ 15. S1 and S2 are high-carbonate alkalinity solutions (≈1M $NaHCO_3$). S3 is an
816 acid solution (pH≈0.63) prepared by dilution of concentrated HCl solution (10%v/v). pH is ex-
817 situ measured at room temperature ≈20°C. Ol: olivinie; Ctl: chrysotile; bru: brucite.

818

819 Table 2. Summary of kinetic parameters for simultaneous serpentinization and aqueous

carbonation of olivine, including alteration of olivine under high carbonate and hydroxyl alkalinity.

Process	$\xi_{extent,\ max}$ (%)	$t_{1/2}$ days	v_0 1/s	R^2
$2Mg_2SiO_4 + 2H_2O + HCO_3^- \rightarrow MgCO_3 + Mg_3Si_2O_5(OH)_4 + OH^-$				
Serpentine formation	65±13	33±13.4	**2.3**x10^{-7}	0.90
Magnesite formation	27±1.7	4.8±1.3	**6.5**x10^{-7}	0.85
Alteration	81±5.2	14±2.5	**6.6**x10^{-7}=1.8636x10^{-9} mol/m^2 s	0.96
$2Mg_2SiO_4 + 3H_2O \rightarrow Mg(OH)_2 + Mg_3Si_2O_5(OH)_4$				
Alteration	105±5.5	2±0.46	**5.9**x10^{-6}=1.6659x10^{-8} mol/m^2 s	0.96
Alteration (initiated in acid pH)	83±7.0*	99±10*	**9.7**x10^{-8**}=2.7389x10^{-10} mol/m^2 s	0.99*

$\xi_{extent,\max}$ is the maximum value of mineral(s) content or alteration extent at apparent equilibrium and $t_{1/2}$ is the half-content time determined by using a kinetic pseudo-second-order model. v_0 is the initial reaction rate ($v_0 = \xi_{extent,\max} / t_{1/2} * 100$). *: values obtained from fitting of a sigmoidal equation ($\xi_{extent} = \xi_{extent,\max} /(1+\exp(-(t-t_{1/2})/b))$). **: effective reaction rate after the so-called incubation period (or induction time) in sigmoidal kinetic behaviors. The alteration rates were normalized with respect to initial specific surface area for olivine fine-grains (2.3 m^2/g).

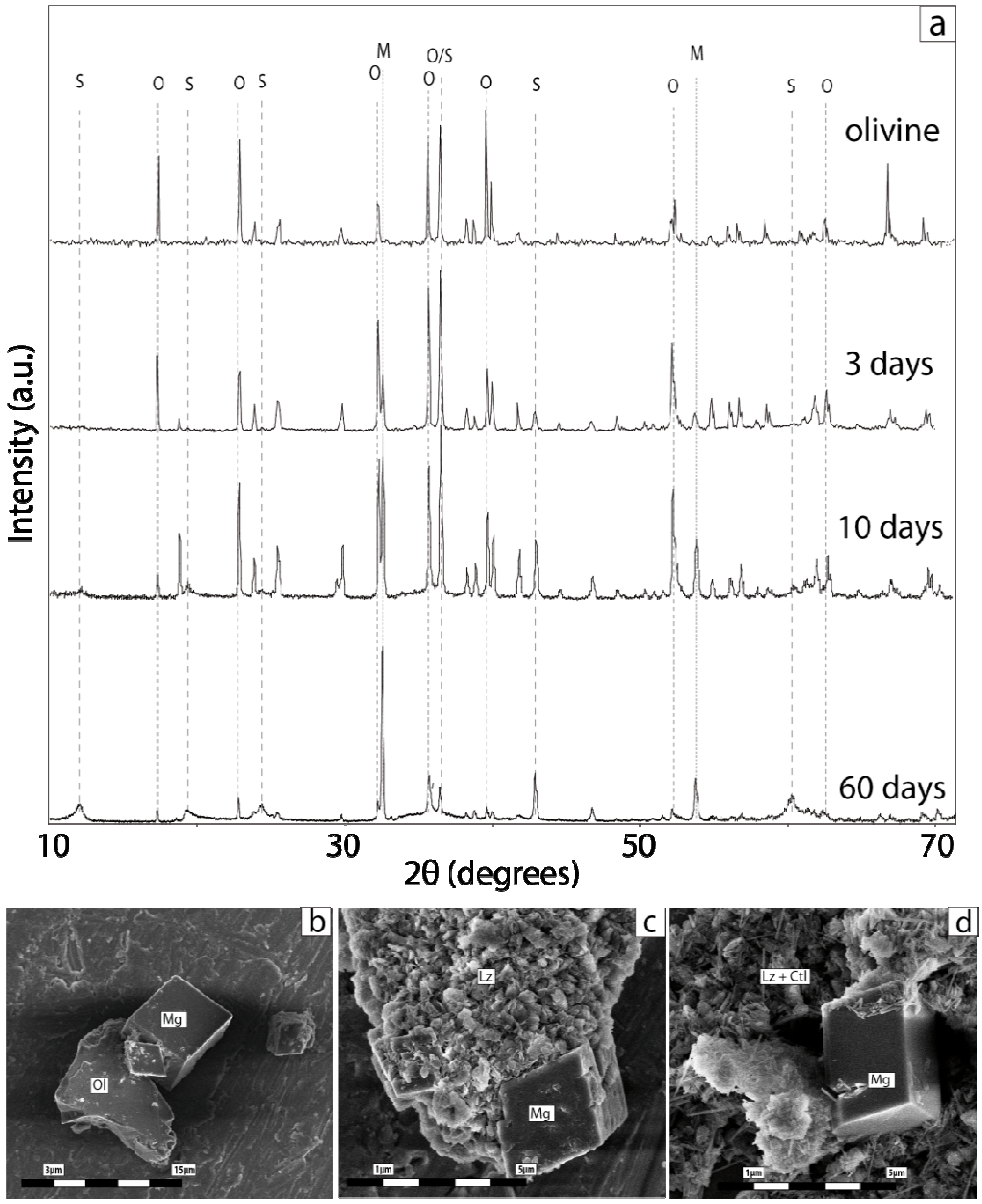

835

836

837 Figure 1. (a) Experimental x-ray diffraction patterns for starting olivine and for products at
838 different reaction time (3 days: run 1; 10 days: run 2 and 60 days: run 5); S: serpentine, O:
839 olivine, M: magnesite. (b), (c) and (d) FESEM images showing the coexistence of magnesite
840 (Mg) and serpentine (lizardite: Lz and chrysotile: Ctl) during olivine (Ol) alteration after 3 days
841 "run 1" (b), 10 days "run 2" (c) and 60 days "run 5" (d).

842

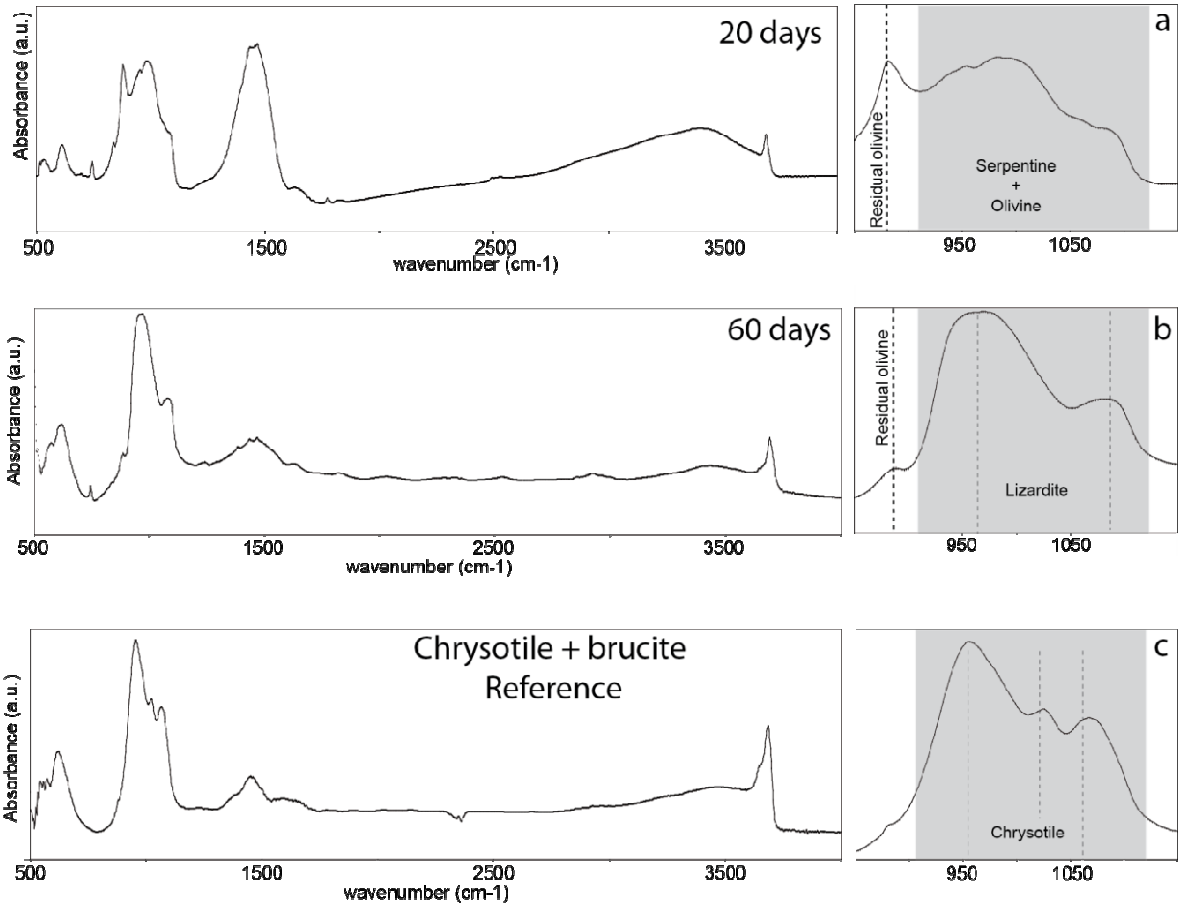

843

844

845

846 Figure 2. Infrared measurements (in transmission option) showing a preferential lizardite
847 formation under high-carbonate alkalinity (panel a “run 3” and b “run 5”) as attested by their two
848 typical stretching infrared modes at 966 and 1085 cm^{-1} for Si-O group (panel b). These infrared
849 features are clearly different to infrared features of chrysotile polymorph (panel c).

850

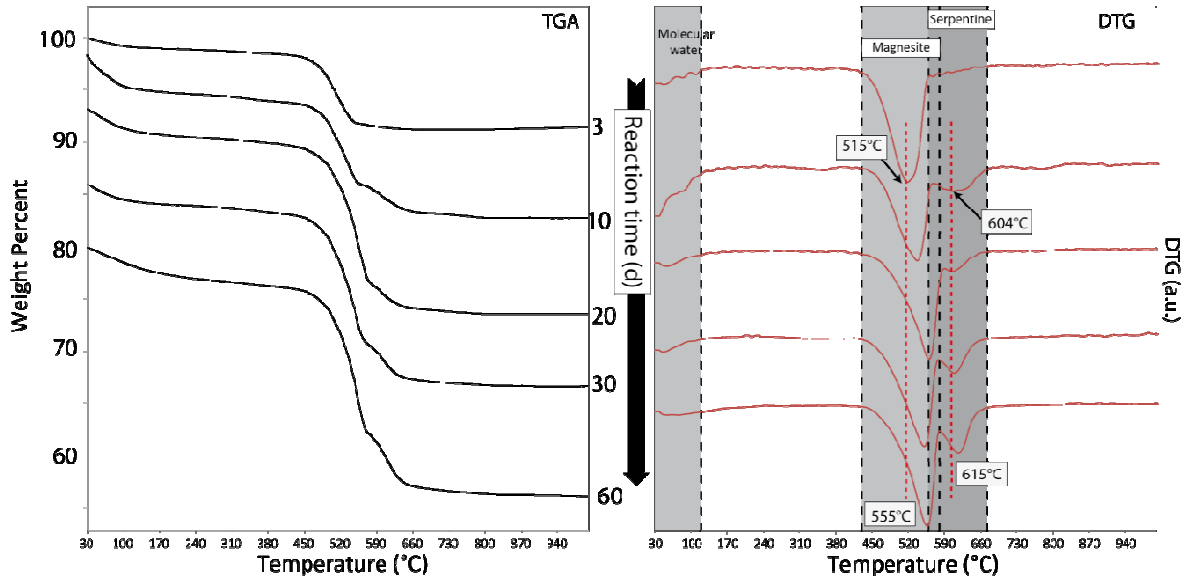

Figure 3. Thermogravimetric analyses (TGA) on the samples collected at different reaction time and its respective 1st derivative curve (DTG) that enables a temporal quantification of coexisting magnesite and serpentine in the samples (runs 1 to 5, see also Table 1 than summarize all TGA values). Magnesite and serpentine decomposition seem to be shifted from 515 to 555°C and from 604 to 615°C, respectively (DTG graphs); probably due to a progressive crystal size evolution and/or mineral proportion.

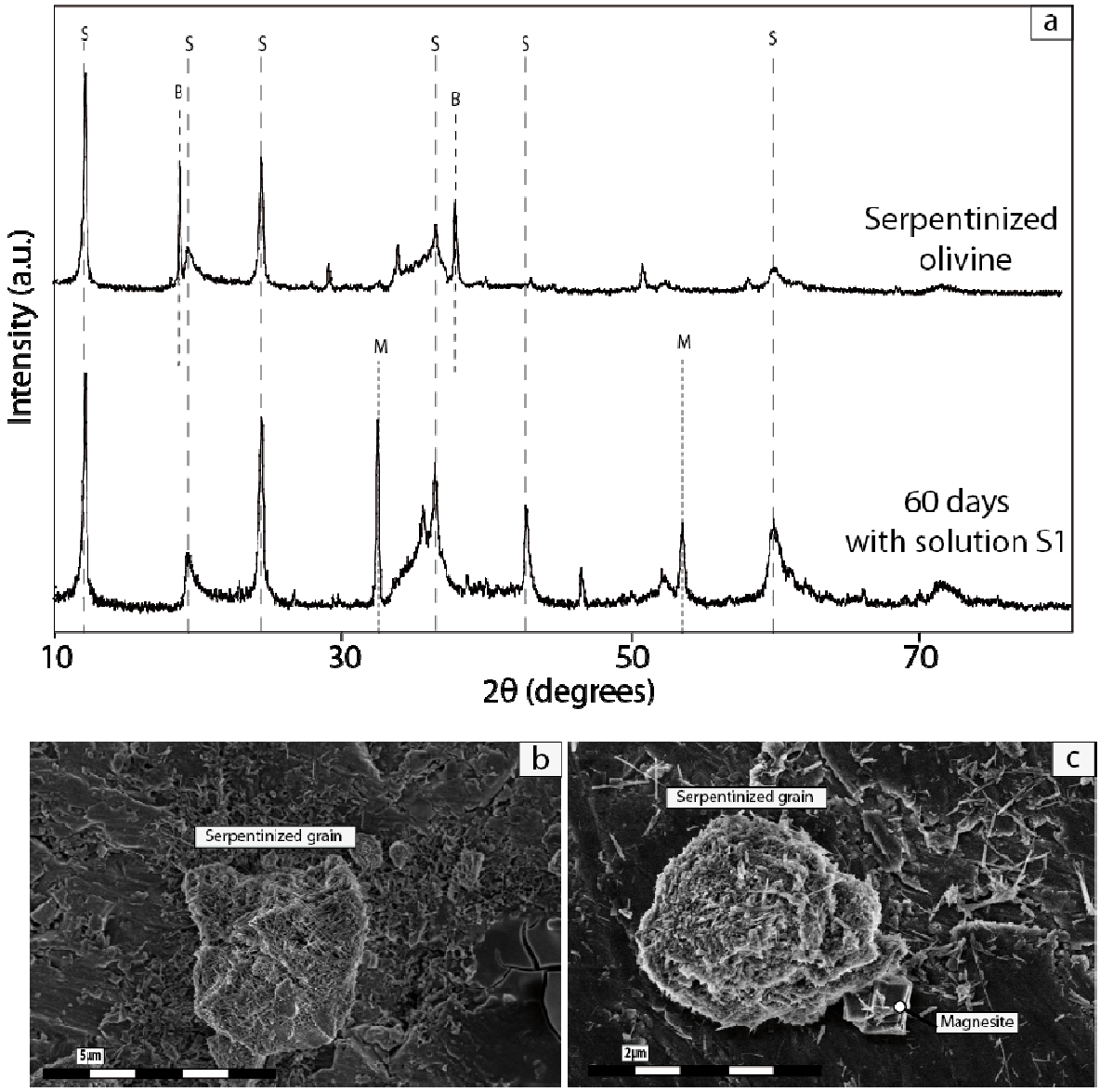

Figure 4. Reactivity of serpentinized olivine (chrysotile+brucite+small amount of residual olivine as starting material) in high-carbonate alkalinity at 200°C. XRD patterns for starting material and after 60 days of reaction (run 15) show only brucite-to-magnesite transformation (a) in agreement with FESEM observations. (b) Starting material and (c) after 60 days of reaction (run 15).

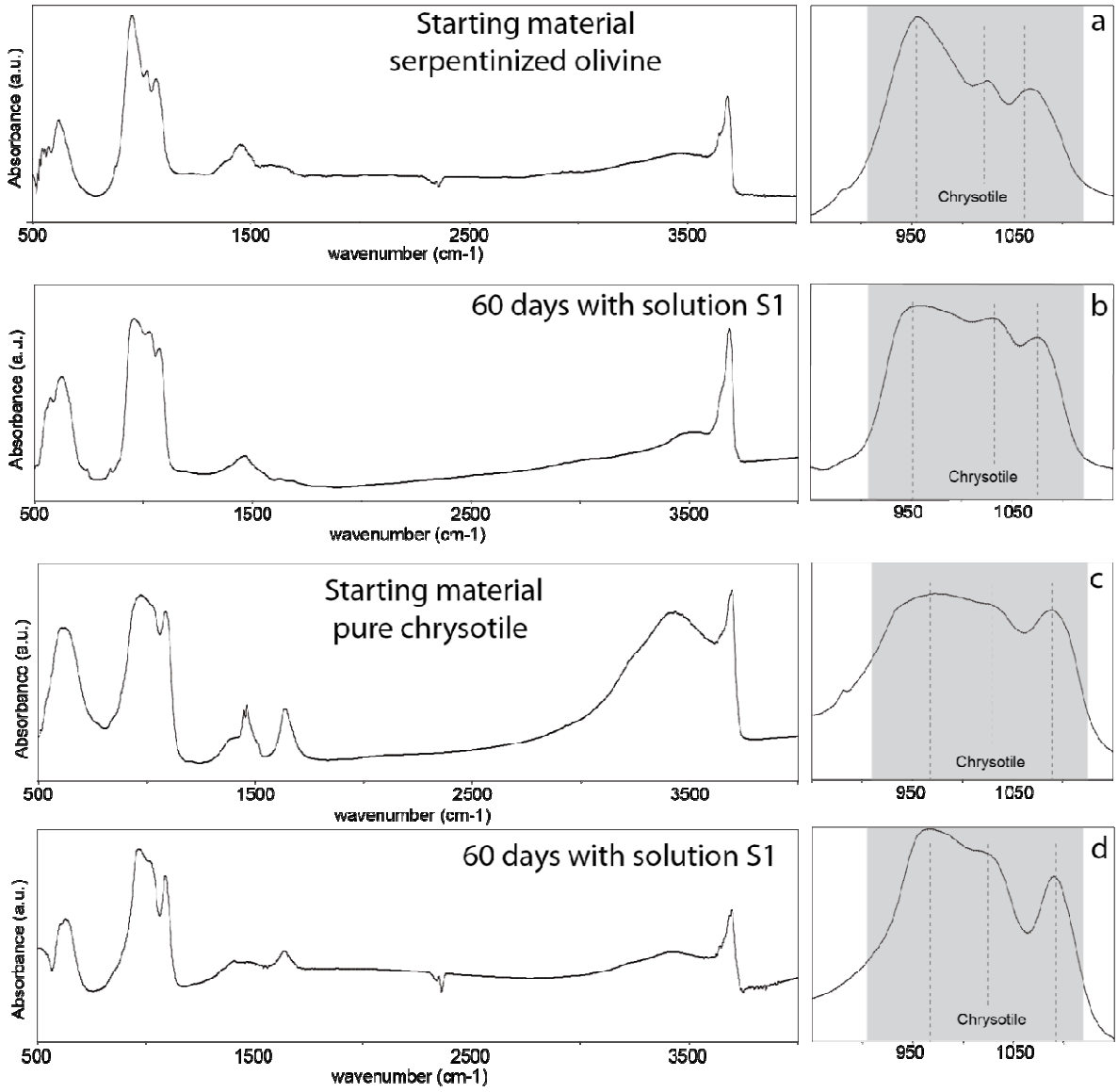

870

871 Figure 5. Infrared measurements confirming slight or insignificant structural changes in reacted
872 chrysotile in high-carbonate alkalinity at 200°C. Two cases, chrysotile contained in the
873 serpentinized olivine (panels: (a): starting material and (b): after 60 days of reaction "run 15")
874 and high-purity synthetic chrysotile (panels: (c): starting material and (d): after 60 days of
875 reaction "run 10").

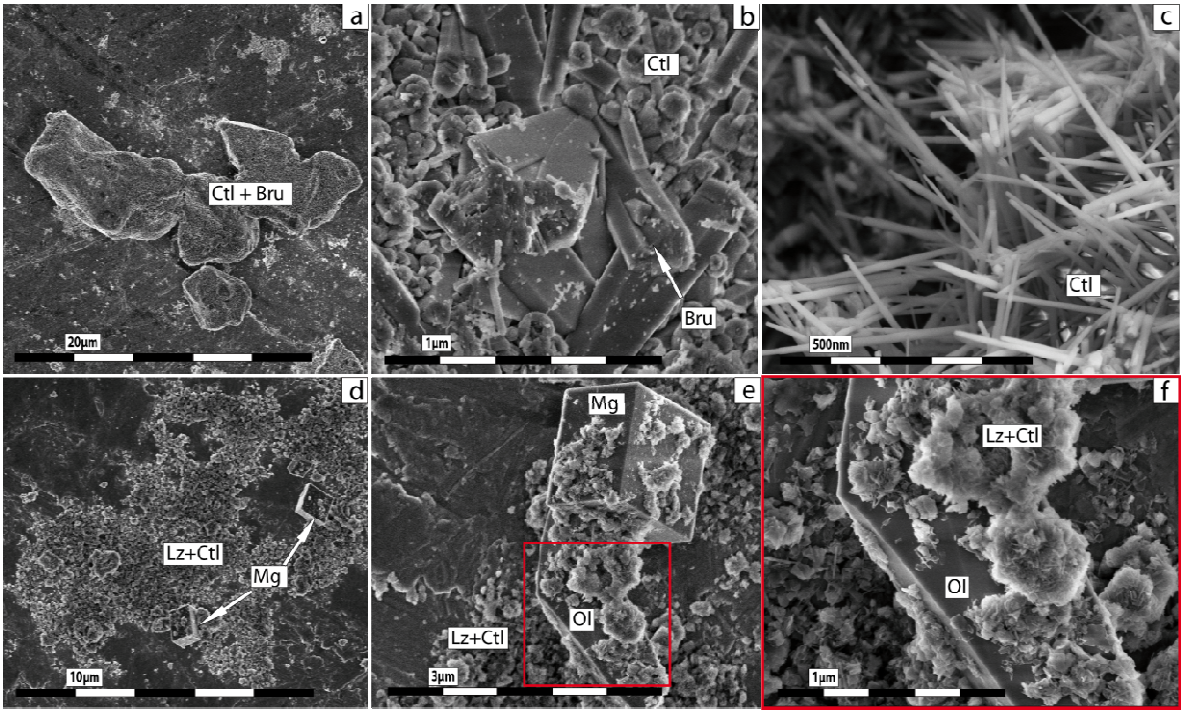

876

877

878

879

880

881 Figure 6. FESEM images: (a), (b) and (c) show mineral replacement of olivine by chrysotile and
882 brucite under high-hydroxyl alkalinity, implying the preservation of original external shape of
883 olivine grains (image (a), see also Lafay et al. 2012). (d), (e) and (f) show the coexistence of
884 magnesite and serpentine precipitation during olivine alteration under high-carbonate alkalinity
885 without preservation of original external shape of olivine grains (run 5).

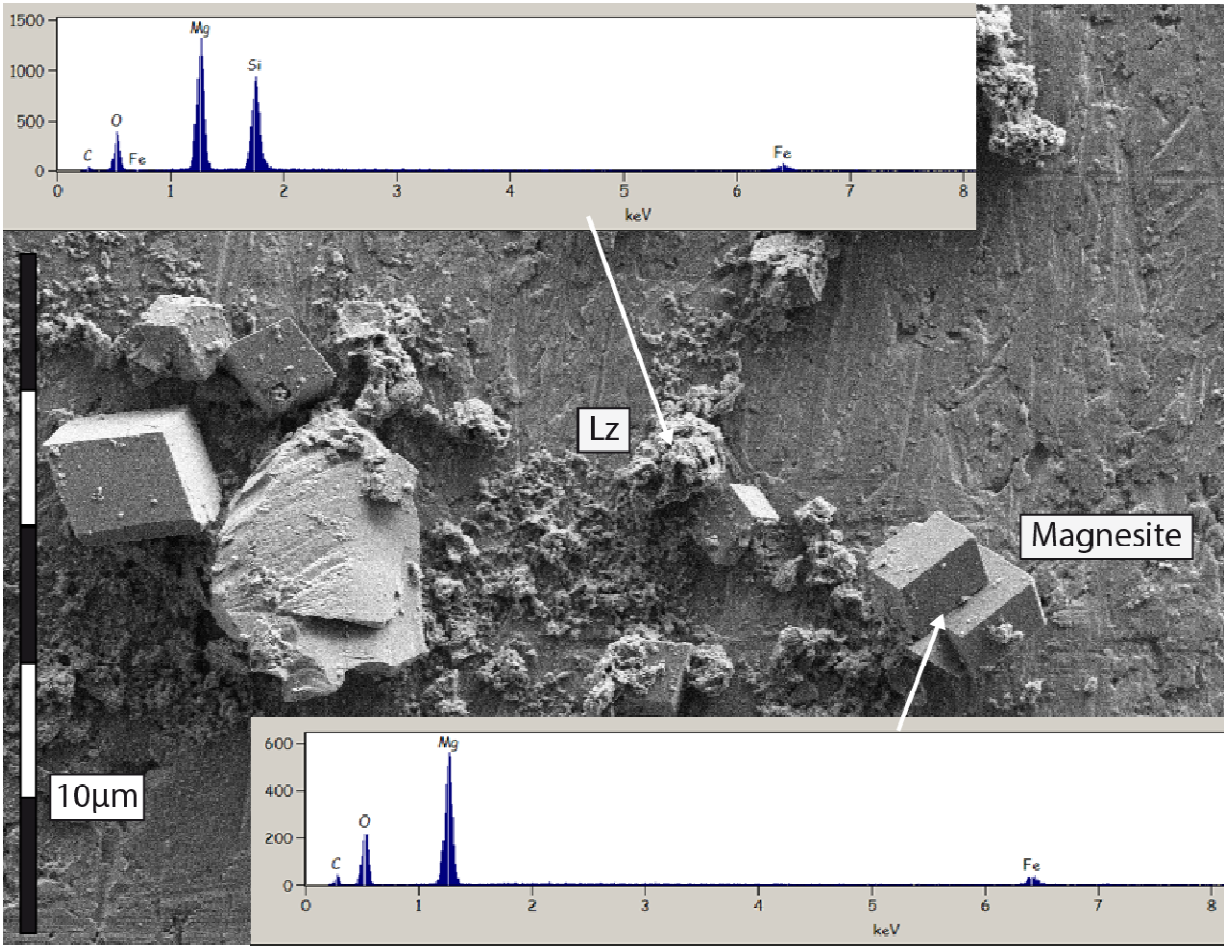

886

887

888

889 Figure 7. FESEM/EDS chemical analyses have revealed complex fate of released iron initially
890 contained in San Carlos olivine. Iron content in magnesite suggests partial iron oxidation via
891 water reduction (sample concerning the run 5).

892

893

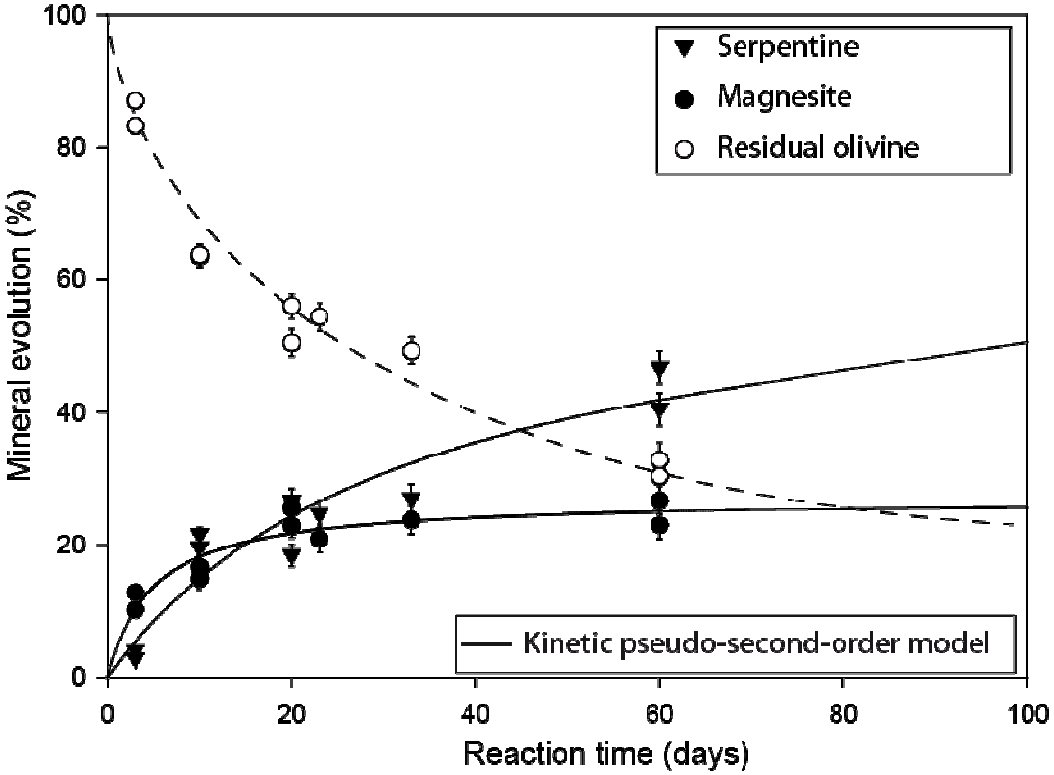

894

895

896 Figure 8. Competitive kinetic behavior of magnesite and serpentine during olivine alteration
897 under high-carbonate alkalinity (runs 1 to 5 and 16 to 20). Experimental kinetic data for
898 magnesite and serpentine were fitted by using a kinetic pseudo-second-order model and kinetic
899 parameters are reported in Table 2.

900

901

902

903

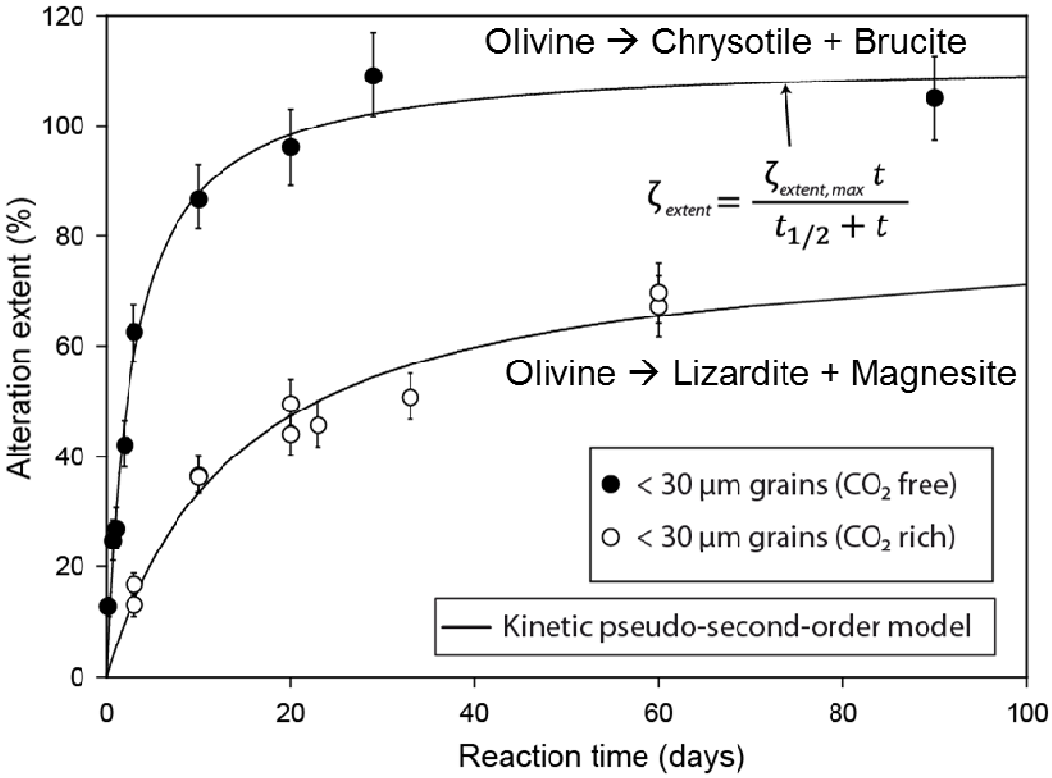

904

905

906

907 Figure 9. Alteration kinetic of olivine under high-hydroxyl alkalinity (circles filled) (from Lafay
908 et al., 2012) and under high-carbonate alkalinity (open circles) (from runs 1 to 5 and 16 to 20).
909 Experimental kinetic data were fitted by using a kinetic pseudo-second-order model and kinetic
910 parameters are reported in Table 2.

911

912

913

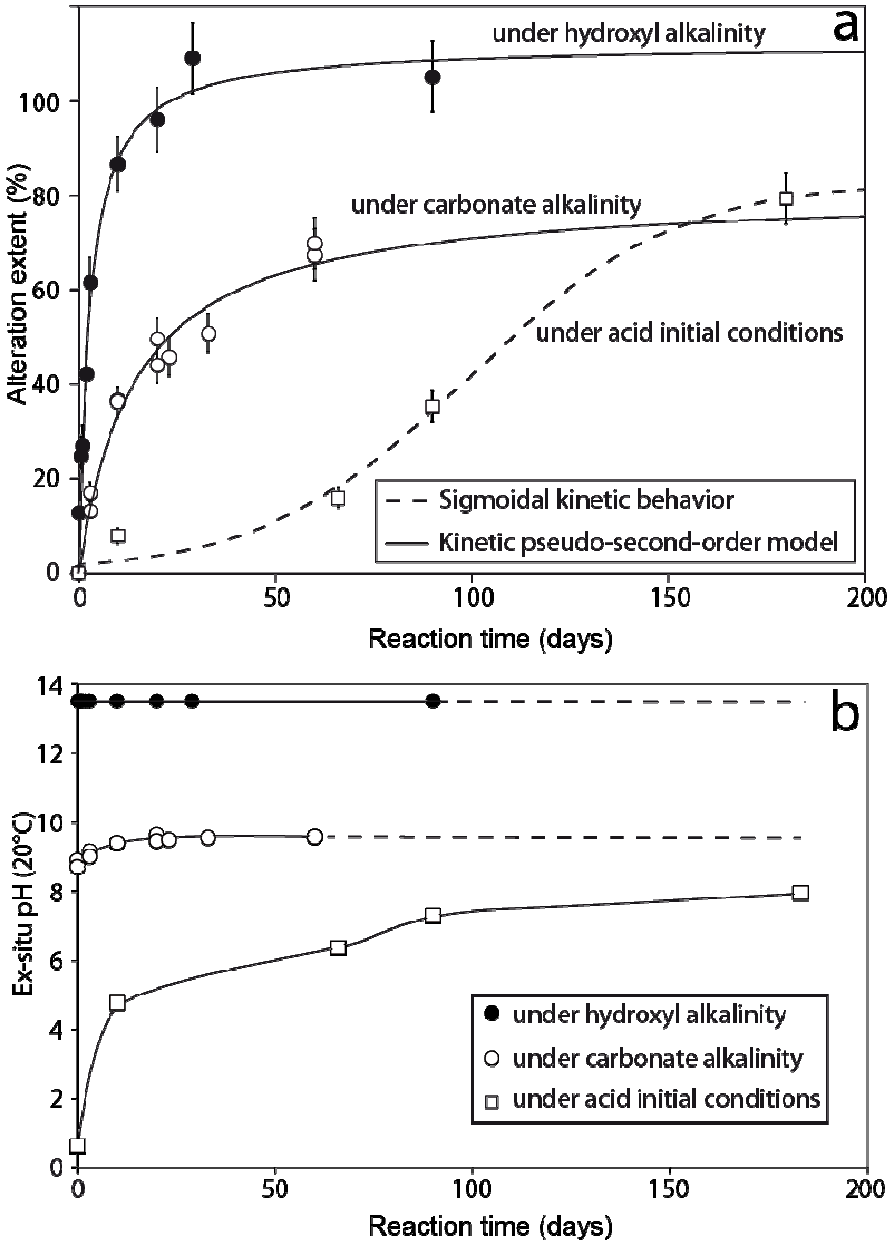

914

915 Figure 10. (a) Alteration kinetic of olivine under high-hydroxyl alkalinity (circles filled) (from
916 Lafay et al. 2012), under high-carbonate alkalinity (open circles) (from runs 1 to 5 and 16 to 20)
917 and initiated in acid pH (open squares) (from runs 21 to 24). (b) pH evolution for each scenario
918 measured ex-situ at room temperature ≈ 20°C.